Contract No:

This document was prepared in conjunction with work accomplished under Contract No. DE-AC09-09SR22505 with the U.S. Department of Energy (DOE) National Nuclear Security Administration (NA).

A Flaw Stability Analysis for the Savannah River Site 3H High-Level-Waste Evaporator – 19548

Charles Keilers, Jr.
Savannah River Remediation

ABSTRACT

The Savannah River Site (SRS) 3H high-level-waste Evaporator (242-25H) entered service in January 2000 and was discovered to be leaking in February 2016. It was robotically repaired and resumed operation in July 2018. During initial restart in December 2017, salt deposits were discovered on the evaporator's lower shell near welds, indicating two more small leak sites. The leak sites have an estimated hydraulic diameter of about 0.1 mm or less – about the diameter of a human hair. The estimated leak rates are about a factor of 10,000 smaller than the robotically repaired leak. An API 579-1/ASME FFS-1 fitness-for-service evaluation determined that if the leak sites are cracks, then they would need to be about 60 mm long (~ 2 inches) to actively and catastrophically grow. Furthermore, a crack of this length would have been detected earlier since it would leak thousands of liters per day. The evaporator was designed with engineered features that minimize risks posed by these small leaks. The path-forward involves operating the evaporator in a deliberate manner with enhanced surveillance. The 3H Evaporator is key to SRS safely and timely reducing its 130 million liter liquid high-level-waste inventory, closing remaining waste tanks, and reducing associated risks to workers, the public, and the environment.

INTRODUCTION

The Savannah River Site (SRS) Liquid Waste System (LWS) safely stores and treats high-level radioactive waste. The LWS consists of 51 waste storage tanks (eight of which are operationally closed and filled with grout), waste evaporators, treatment facilities, and solidification facilities, such as the Defense Waste Processing Facility (DWPF) and Saltstone Production Facility (SPF). During the last sixty years, SRS tank farms have received about 600 million liters of high-level-waste (HLW). A series of evaporators have reduced the waste volume by about a factor of four, to about 130 million liters (i.e., 35 million gallons) [1]-[4]. The remaining waste is stored in tanks that are up to about seven decades old. The 3H Evaporator has a key role in SRS safely and timely reducing this liquid waste inventory, closing the remaining HLW tanks, and reducing the associated risks to workers, the public, and the environment.

Since 1996, SRS has also been vitrifying HLW at the Defense Waste Processing Facility (DWPF). DWPF has encapsulated waste in glass in approximately 4,100 stainless-steel one-ton canisters, with a projected 4,000 or so to go. A key step for preparing DWPF feed is sludge batch washing. This is a batch process involving adding inhibited water to a selected HLW tank to remove dissolved solids, allowing solids to settle, and then transferring the sludge to DWPF. DWPF combines the sludge with other waste streams and with borosilicate glass frit. The mixture is then melted and poured into the stainless-steel canisters. The canisters are stored in below-grade concrete vaults until final disposition. During the process, DWPF generates a "recycle" liquid waste stream that is returned to the tank farms.

SRS currently has two operational HLW evaporators to manage liquid waste volume. The 2H Evaporator (242-16H) manages the DWPF recycle stream. The 3H Evaporator is newer, about four times larger in volume, and manages the rest, particularly the decant from sludge batch washing.

In 2016, the 3H Evaporator vessel was discovered to be leaking, and in 2017, it was remotely repaired [5]-[8]. Leakage was captured in the below-grade stainless-steel lined evaporator cell, preventing a hazard to personnel and a release to the environment. The time needed for repair did not affect overall liquid waste operations for two reasons: (1) a qualified sludge batch had just been prepared that could feed DWPF for several years; (2) a DWPF melter electrode failed in 2017, after nearly 14 years of operation; this was anticipated and warranted a melter replacement outage in parallel with the 3H repair [9].

In December 2017, during 3H restart, salt deposits were discovered on the lower shell, indicating two more leak sites (Figure 1). The north leak site manifested itself as a small salt nodule at a weld intersection; the south leak site has a visible salt streak at a meridional weld. Estimated maximum leak rates are about 0.5 L/day, which is about a factor of 10,000 smaller than the leak repaired in 2017.

A System Engineering Evaluation (SEE) explored options to address the newly discovered leak sites, including repair, replacement, new technology, single evaporator operation (2H), and use of 3H as-is with "Enhanced Surveillance." Factors considered included but were not limited to cost, schedule, worker radiation exposure, the short and long-term risks, and how well the risks could be managed. All the options required a period of 3H operation, as-is, if DWPF is to continue to reduce risks by encapsulating HLW without a possibly multiyear interruption. The 3H Evaporator has engineered features that could minimize the risk posed by such operation, including the stainless-steel lined concrete cell; a continuously monitored cell sump; HEPA-filtered and monitored active ventilation; and a monitored cell under-liner.

The Enhanced Surveillance option was chosen because it appropriately balances the minimal risk posed by small, well-controlled releases of waste into the evaporator cell verses the potential long-term risks from extending storage in aging HLW tanks.

Among numerous considerations in the resumption decision was fitness-for-service. This paper summarizes the API 579-1/ASME FFS-1, *Fitness for Service*, evaluation performed before resuming to assess the potential for unstable crack growth in the evaporator shell [13].

DESCRIPTION

The 3H Evaporator is a single-stage "pot" evaporator, about 8 meters tall by 4 meters diameter (Figure 1). It is functionally identical to earlier SRS evaporators but about four times larger in volume and more corrosion-resistant. The vessel consists of a lower conical section supported by four legs, an upper cylindrical section with a horizontal steam tube bundle, and a vessel head. The vessel operates near atmospheric pressure; heat from the tube bundle concentrates the highly caustic liquid waste.[1] Operating parameters are continuously monitored such that an upset leading to an abnormal condition would cause an alarm and be addressed. References [5], [6], and [8] further describe the evaporator and its operation.

Evaporator components exposed to waste are made from Alloy G-3 (UNS N06985), an austenitic nickel-based alloy with low corrosion susceptibility in waste [8], [10]-[12]. This evaluation uses stainless steel fracture toughness properties since Alloy G-3 strengths generally exceed those for stainless steels.[2]

---

[1] The vessel design basis is 200ºC; pressures of 0.1 MPa (15 psig) and full vacuum; and liquid specific gravity (SpG) of 1.7. The bottom head has about a factor of fifty margin against internal pressure ([18], Section UG-32e).

[2] Alloy G-3 (SB-582) minimum design yield and tensile strengths are about 17% and 20% greater than those for stainless steel 304 (SA-240).

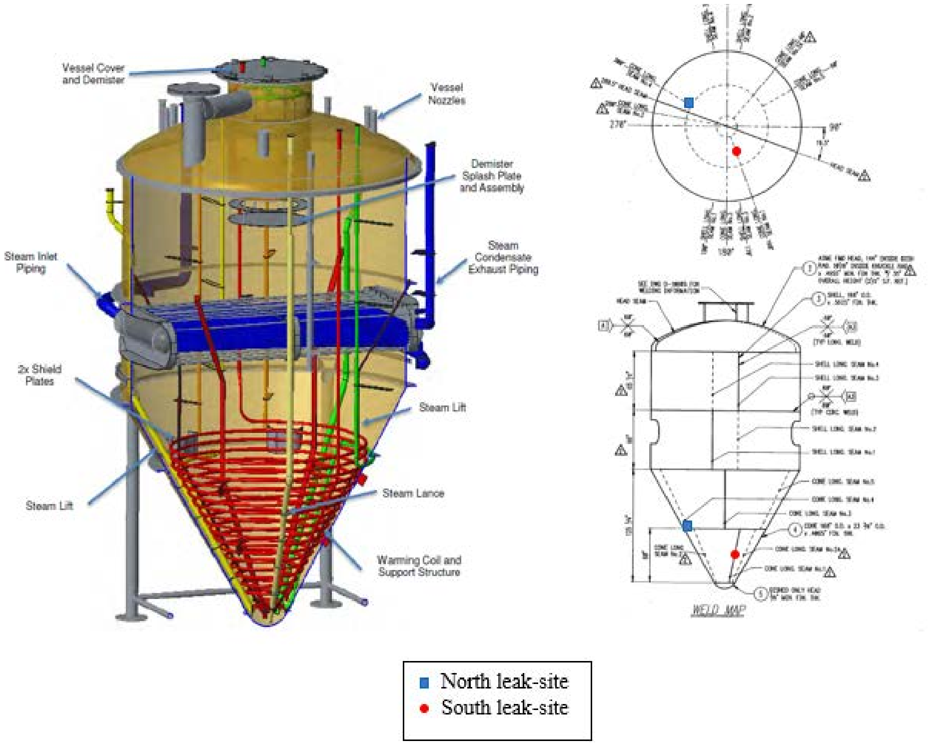

Figure 1. Major components of the 25H Evaporator [6], and the December 2017 leak locations.

LEAKAGE HISTORY AND ESTIMATED FLAW SIZE

In February 2016, the 3H evaporator shell was discovered to be leaking at a maximum rate of about 600 L/day. Remote cell inspections showed extensive salt deposits coming from where the vessel legs join the support ring and penetrate the insulation sheathing [5]-[6].

During 2016 and 2017, insulation and sheathing on the evaporator's lower shell were robotically removed. Multiple leak sites were discovered at the bottom head, due to erosion [8]. Estimated leak rate without insulation was roughly 5,000 L/day with liquid at operating level. The shell was robotically repaired [7]. Insulation was not restored because of high radiation levels and acceptable thermal conditions.

Shortly after resuming, salt deposits were discovered at two locations near welds on the conical vessel. During most of 2017, the evaporator was either empty or had liquid with SpG of 1.0, which would leave little visible salt residue. With heat-up, liquid waste concentrates, and boiling temperature and viscosity both increase. Leak-rate decreases as viscosity increases, but salt residue becomes readily apparent.

Projected leak rates are about 0.5 L/day or less, based on visible salt released over a known period. Estimated equivalent hydraulic diameters are about 0.1 mm or less – roughly the diameter of a human hair.[3] It isn't definitively known that the leak-sites are cracks. However, if they are, an equivalent crack, with aspect ratio of 20, would be about 0.03 mm wide by 0.6 mm long.

---

[3] Equivalent hydraulic diameters were estimated using Bernoulli's equation for laminar flow through either a hole or a crack, with pressure drops due to viscosity and surface tension.

YIELD STRESSES AND RESIDUAL WELD STRESSES

Yield and residual stresses turn out to be key to this evaluation. API 579-1/FFS-1 uses actual or nominal values of yield and tensile strengths for fitness-for-service evaluations and has adjustments for operating temperature.[4] For the 3H Evaporator at temperature (200 ^{o}C):

- Minimum yield stress (σ_y) is 233 MPa (33.8 ksi).
- Maximum yield stress is 246 MPa (35.7 ksi) or 1.06 σ_y.
- Minimum ultimate tensile stress 572 MPa (82.9 ksi) or 2.45 σ_y.

Plastic flow stress is the average of yield and tensile stresses (i.e. 1.73 σ_y).[5] Without cracking, the API 579-1/FFS-1 criteria avoid plastic failure by ensuring that primary (i.e., load-carrying) stresses do not exceed 1.8 times yield stress, which is approximately the plastic flow stress.

API 579-1/FFS-1 uses yield stress to estimate weld residual stresses.[6] Since the 3H vessel is made of a nickel-based alloy, the vessel was not post-weld heat treated.[7] Hydrostatic test pressure was also too low to relieve residual stresses. Therefore, for the 3H Evaporator, the residual stresses are taken to be the same as the maximum yield stress, which is 1.06 σ_y.

OVERVIEW OF FRACTURE MECHANICS

Fracture mechanics can predict the flaw size that would induce unstable crack growth. Figure 2 shows the configuration. Linear elastic fracture mechanics predicts the following principal stresses near the crack-tip on the *x*-axis, if tensile forces are perpendicular to the crack:[8]

$$\sigma_{xx}(x) = \sigma_{yy}(x) = \frac{K_I}{\sqrt{2\,\pi\,x}} \tag{1}$$

Where K_I is a *stress intensity factor* (units of MPa-m^{½}), and x is the distance from the crack tip. Equation (2) and K_I are commonly used to relate the local stresses at the crack tip, which drive crack growth, to the global stress field in a structure in the absence of a crack.

$$K_I \equiv G\,\sigma_g\,\sqrt{\pi\,c} \tag{2}$$

Where:

- σ_g is the global stress perpendicular to the crack surface in the absence of the crack.
- c is half the crack length.
- G generically represents several adjustments given in [13] for particular geometries. For this evaluation, given the small flaw size, G will be taken to be 1.05.

---

[4] Reference [13], Sec. 9.4.3.2, Step 3; Sec. 9.3.5.1; Annex 2E, Sec. 2E.2.1.

[5] Reference [13], Annex 2E, Section 2E.2.2.2.a..

[6] Reference [13], Annex 9D, Sec. 9D.3.3 and 9D.5 and 9D.6.

[7] Reference [18], Sec. UNF-56.

[8] Reference [14] equation 2.39. K_I is commonly referred to as the "Mode I" stress intensity factor and is due to loads with mirror-symmetry about the crack. Modes II and III have asymmetric loading in the crack's plane.

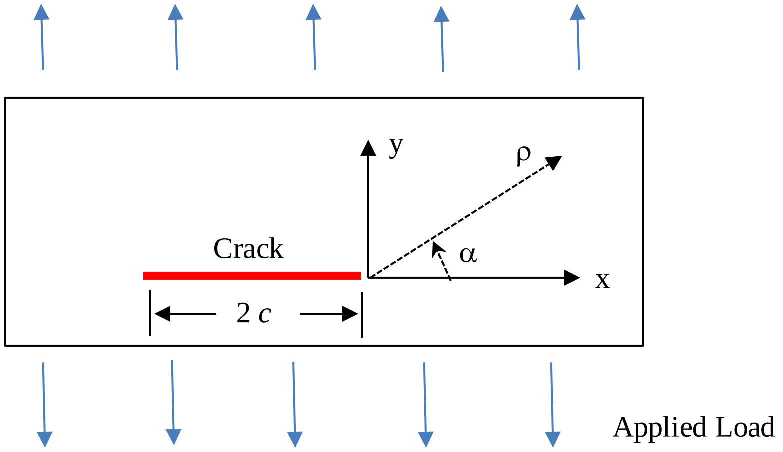

Figure 2. Through-wall crack and load geometry and coordinate system.

Creating a free surface requires energy to do work, similar to machining a part.[9] Cracks can spontaneously grow if the strain energy released exceeds the work required to create a free surface.[10] A common criterion for crack growth is when K_I exceeds a critical limit, K_{mat}. Reference [13] suggests K_{mat} of 132 MPa-m^{½} for austenitic stainless-steel weldments, which is applied here to Alloy G-3.[11]

Equation (1) predicts an unrealistic singularity and infinite stresses at the crack tip. Instead, a blunted plastic zone develops at the crack tip. Equation (2) can account for the plastic zone by assuming a slightly longer crack. The through-wall crack configuration in plane stress has an effective stress intensity factor:[12]

$$K^{eff} = \Phi\, K^{SR} = \Phi\left(G\, \sigma^{SR} \sqrt{\pi\, c}\right) \quad \text{where } \Phi \equiv 1 \Big/ \left[1 - \frac{1}{2}\left(\frac{\sigma^{SR}}{\sigma_y}\right)^2\right]^{1/2} \tag{3}$$

and:

- σ_y is minimum yield stress.
- σ^{SR} is the sum of secondary and weld residual stresses.
- K^{SR} is the stress intensity factor due to secondary and residual stresses.
- Φ is the plasticity interaction factor.

The leak-sites are far from discontinuities, such as the top of the cone, the bottom head, and an anti-buckling stiffener midway down the cone. These discontinuities will have secondary stresses that decay exponentially with distance.[13] Consequently, $\sigma^{SR} = 1.06\ \sigma_y$, and by Equation (3), the plasticity interaction factor Φ is about 1.5. σ^{SR} turns out to be about six times larger than its counterpart for primary stresses (σ^P). Therefore, the weld residual stresses are the dominant factor influencing unstable crack growth.

---

[9] https://en.wikipedia.org/wiki/Surface_energy

[10] Alan Griffith (1920), George Irwin (1948), and Egon Orowan (1948) developed this model, including plasticity effects. More details can be found in [14] and at the website: http://www.fracturemechanics.org/griffith.html

[11] Reference [13], Annex 9F.4.8.2, suggests 132 MPa-m^{½}, for austenitic stainless steel weld material, which is 60% of the value suggested by [13] for the base metal of the same material.

[12] Reference [14], Equation (2.70). Reference [13], Sec. 9.4.3.2, Step 10 is approximately equivalent to Equation (3) for small flaws. API 579-1/ASME FFS-1 also applies Φ only to the sum of the secondary and residual stresses.

[13] Reference [16], equation (96); Reference [17], Equation (278).

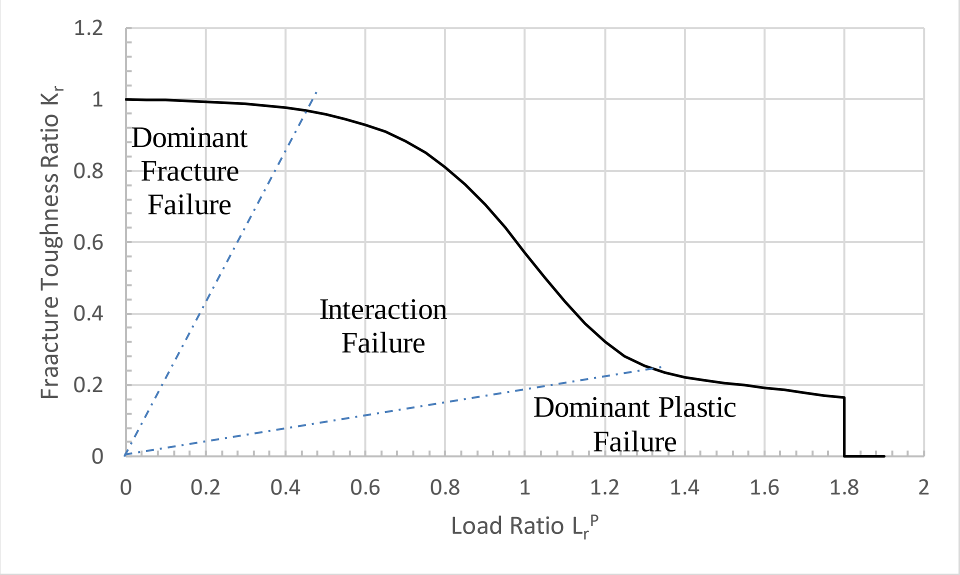

Figure 3: Failure Assessment Diagram (FAD) for austenitic stainless steels [13].

CRACK STABILITY EVALUATION

The API 579-1/FFS-1 Level 2 procedure was used for the 3H Evaporator.[14] It starts with a known or assumed half-crack-length, c, yield stress, σ_y, and fracture toughness K_{mat}. Early steps identify:

- Primary stresses, σ^P, which balance the external loads.
- Adjusted primary stress intensity factors, $K^P = G\,\sigma^P\,\sqrt{\pi\,c}$.
- The load ratio, $L_r = G\,\sigma^P / \sigma_y$, based on maximum principal stress and minimum yield stress.

The later steps identify:

- The secondary and residual stresses, σ^{SR}.
- Adjusted secondary and residual stress intensity factors, $K^{SR} = G\,\sigma^{SR}\,\sqrt{\pi\,c}$.
- The plasticity interaction factor Φ.
- The fracture toughness ratio K_r, which is defined as $(K^P + \Phi\,K^{SR})/K_{mat}$.

K_r and L_r are then plotted on a Failure Assessment Diagram (FAD), such as Figure 3. The FAD accounts for the potential for interaction between failure by cracking and failure by plastic instability. A stable crack has a (L_r, K_r) point that falls below and to the left of the limit curve. Figure 3 shows the limit curve that is recommended when a stress-strain curve is not available:[15]

$$K_r^{limit} = (1 - 0.14\,L_r^2)\,[0.3 + 0.7\exp(-0.65\,L_r^6)] \qquad \text{for } L_r \le 1.8 \qquad (4)$$

References [13] suggests a cut-off of 1.8 for austenitic stainless steels, which is also approximately the ratio of plastic flow to yield stress for Alloy G-3.

---

[14] Reference [13], Section 9.4.3.

[15] Reference [13], Section 9.4.3.2, Step 12 and Figure 9.19. Reference [14], Equation (9.68a).

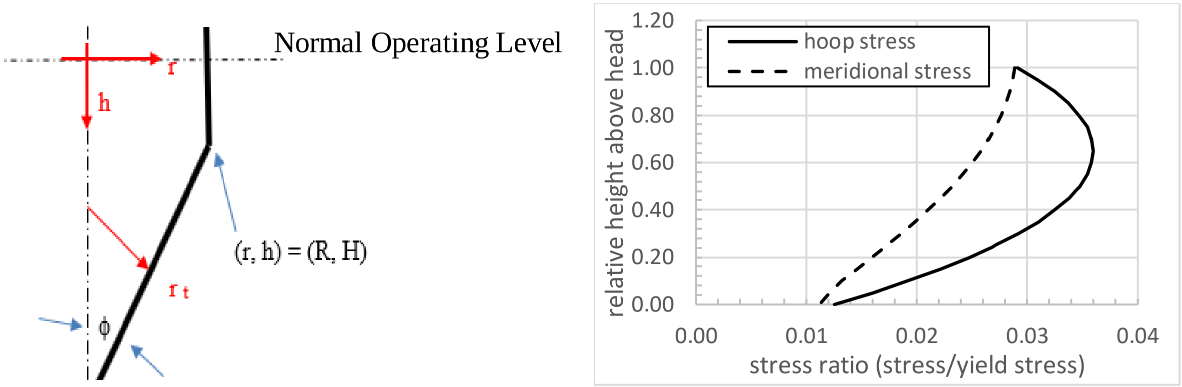

Figure 4. Coordinate system and ratios of non-seismic primary stresses to yield stress. The semi-apex angle ϕ is 30°. The tangential radius, r_t, is given by $r_t = r / \cos(\phi)$.

The Level 2 approach is deliberate but intended to apply to a wide range of situations. These include thin or thick flat plates, cylinders, or spheres that are designed to code; not operating in the creep range; have insignificant dynamic loads; and have one of a variety of pre-analyzed crack-like geometries. Fundamentally, the problem it solves is: given loads, material data, and flaw size, find K_r and L_r.

Alternatively, for a thin shell and through-wall crack, the relations presented can be used to solve the inverse problem: given L_r and a “target K_r,” find the critical half-crack-length c_{limit} for unstable growth.[16]

A procedure to estimate the critical crack length under these simplified conditions is as follows:

1. Use the fracture toughness for austenitic stainless-steel weldments: K_{mat} = 132 MPa-m^{½}.

2. Determine the primary stresses, σ^P. The evaluated loads are liquid pressure at temperature, and metal weights.[17] Figure 4 shows the maximum non-seismic primary stress is about 0.035 σ_y. If one includes a seismic contribution (which is determined separately and is localized), then the stress ratio σ^P/σ_y increases to 0.18.

3. Determine the load ratio, $L_r = G\, \sigma^P / \sigma_y = 0.19$, where G is assumed to be 1.05.[18]

4. Use L_r and Equation (4) to determine the target fracture toughness ratio, $K_r = 0.99$. Interaction with plastic instability is negligible.

---

[16] The shell thickness is about 8.7 mm. At the leak-site elevations, the radius-to-thickness ratios are about 84.7 and 136 for the south and north leak-sites, respectively.

[17] Reference [16], Equations (52) and (53), present the equilibrium equations. The tangential equilibrium equation for a cone is the same as for a right cylinder if the tangential radius r_t in Figure 4 replaces the radius r. See also, Reference [18], UG-32(f).

[18] G represents several adjustments in Reference [13]; a detailed evaluation found they are bounded by 1.05.

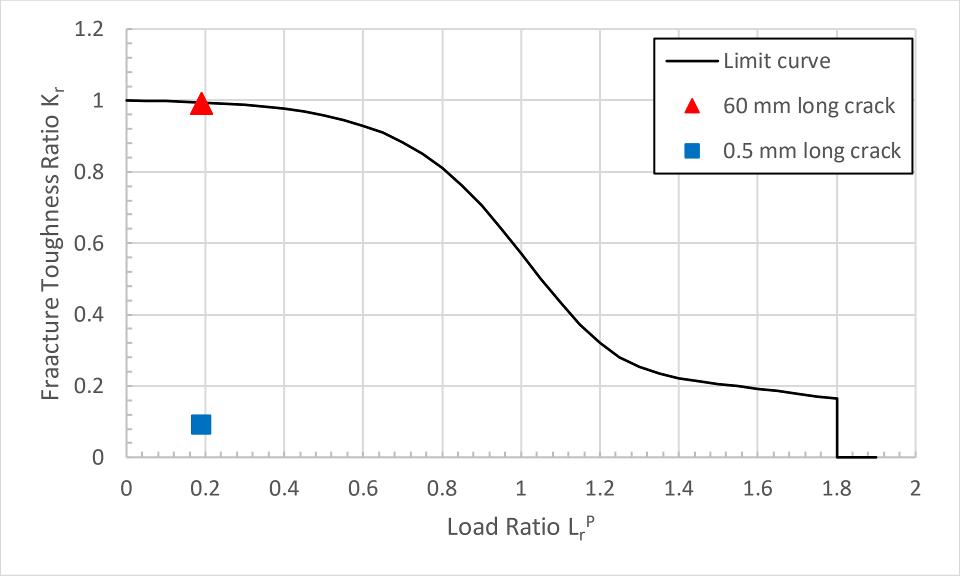

Figure 5. Failure Assessment Diagram (FAD) with results for two crack lengths.

5. Estimate the sum of the secondary and residual stresses, as previously discussed. The stress ratio $\sigma^{SR}/\sigma_y = 1.06$, which is six times larger than the primary stress ratio, $\sigma^P/\sigma_y = 0.19$.

6. Determine the plasticity interaction factor using the stress ratio σ^{SR}/σ_y and Equation (3): $\Phi = 1.5$.

7. Solve for c_{limit} – the half-crack-length above which crack growth becomes unstable.

    a. Define a global stress: $\sigma \equiv (\sigma^P + \Phi\sigma^{SR}) = 1.78\ \sigma_y = 415$ MPa.

    b. Recognize that, for small cracks, the fracture toughness ratio is:

    $$K_r \equiv \frac{1}{K_{mat}}(K^P + \Phi K^{SR}) \cong \frac{1}{K_{mat}}\ G\,\sigma\sqrt{\pi\, c} \qquad (5)$$

    c. Then, the limiting crack length is:

    $$2 \cdot c_{limit} = \frac{2}{\pi}\left[\frac{K_r\ K_{mat}}{G\,\sigma}\right]^2 \cong 60\text{ mm (~ 2 inches)} \qquad (6)$$

8. *Conclusion:* The estimated critical crack length (2 c_{limit}) is about 60 mm. This is about two orders of magnitude larger than the estimated flaw length (~ 0.6 mm).

Alternatively, one could use Equation (5) to calculate the fracture toughness ratio K_r, based on the estimated flaw-length: $2\ c = 0.6$ mm. The result is $K_r = 0.1$. Figure 5 shows the FAD for the estimated flaw and the critical flaw lengths.

ESTIMATED LEAK RATE FROM CRITICAL-LENGTH CRACK

During most of 2017, the 3H Evaporator was either empty or had sufficient water to achieve about 10 to 40 kPa pressure at the leak-sites. The discussion below shows that the leak rate from a 60-mm long crack in the 3H Evaporator lower shell would be readily detectable over this pressure range.

Assume a long crack, with length *L* much greater than width *w*. Hydraulic diameter is defined as [19]:

$$d = (4)(\text{flow area})/(\text{perimeter}) \cong 2 \cdot w \tag{7}$$

To estimate the width, consider that plastic deformation blunts the tip of a crack. In fact, the width across the crack-tip, the *crack-tip opening displacement (CTOD),* is used as a metric in fracture mechanics for plasticity effects. Using CTOD as an estimate for average crack width (*w*) will lead to a lower estimated flowrate, since most of the crack has greater width. From fracture mechanics for plane stress, CTOD is:[19]

$$w \approx CTOD = \frac{K_I^2}{\sigma_y E} \quad \text{where } E \text{ is Young's Modulus, 182 GPa for Alloy G3.} \tag{8}$$

If $K_I = K_{mat}$ (132 MPa-m^{½}), the crack width and hydraulic diameter are: $w = 0.4$ mm and $d = 0.8$ mm.

For water at 20 °C, the kinematic viscosity is $v = 1 \times 10^{-6}$ m^2/s. Reynold's number is defined as [20]:

$$Re = \frac{V\,d}{v} \cong \frac{2\,Q}{v\,L} \text{ for a long crack or } Q \cong \frac{1}{2} Re\, v\, L \tag{9}$$

Where *L*, *V*, and *Q* are the crack length (60 mm), bulk velocity (m/s), and flow-rate (m^3/s), respectively. For a pipe or channel, the flow is laminar if $Re \leq 2{,}300$ [20]. Using equation (9), the maximum flow that could still be laminar for a 60-mm crack is about 6,000 L/day (~1,600 gal/day). This would be readily detectable.

Bernoulli's Equation with friction losses gives the relationship between pressure and flow [20].

$$\Delta P = \frac{1}{2}\rho V^2 \left(1 + f\frac{h}{d}\right) = 2\frac{\rho\, Q^2}{d^2\, L^2}\left(1 + f\,\frac{h}{d}\right) \tag{10}$$

Where ρ is the fluid density (1,000 kg/m^3), h is the wall thickness (8.7 mm), and f is the Darcy-Weisbach friction factor. For laminar flow between parallel plates, $f = \frac{96}{Re} = 0.04$ maximum.[20] At higher turbulent flows through a crack with rough internal surfaces, assume $f = 0.1$.[21]

Figure 6 plots the calculated leak rates for pressures in the range of 10 to 40 kPa. Flow is turbulent throughout this range. Leak rates for a critical length crack range from 6,000 to 13,000 L/day (1,600 to 3,400 gal/day) and would be readily detectable.

---

[19] Reference [14], Equation (3.8), plane stress conditions.

[20] Reference [19], assuming laminar plane Poiseuille flow.

[21] Reference [20], Figure 8.14: 0.1 is an upper-bound friction factor for fully developed flow in circular pipes.

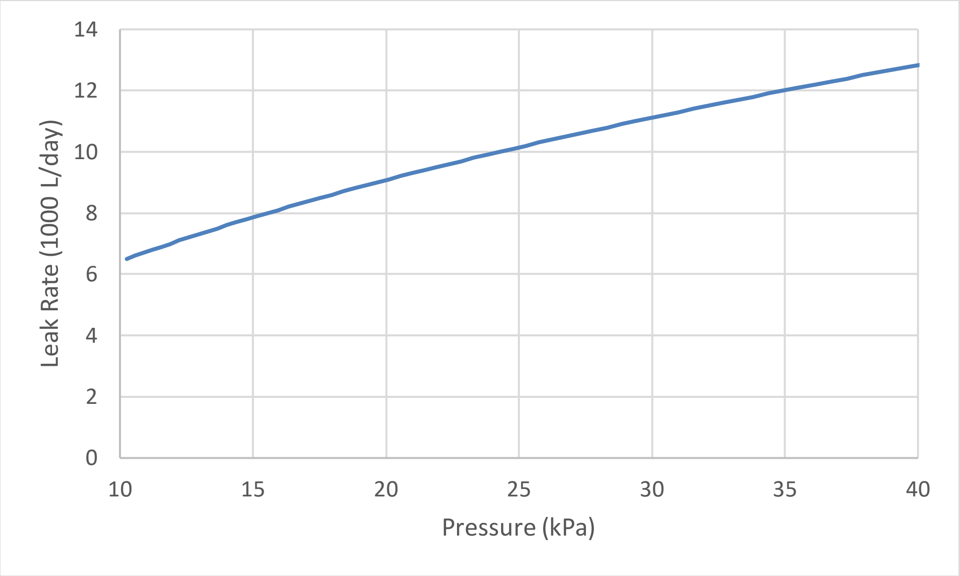

Figure 6. Calculated leak rates for a 60-mm long crack for the pressure range of 10 – 40 kPa.

CURRENT STATUS

The SRS 3H Evaporator resumed operation in July 2018 in a deliberate manner with enhanced surveillance due to two newly discovered leak-sites near welds on the conical shell, with estimated leak rates of 0.5 L/day or less.

CONCLUSIONS

This paper summarizes a fitness-for-service evaluation for unstable crack growth in the 3H Evaporator using the approach in API 579-1/ASME FFS-1 (Reference [13]). Key conclusions are:

- Based on visible salt deposits, the equivalent hydraulic diameter of the leak sites is about 0.1 mm or less, which is about the diameter of a human hair.
- It's not clear that the leak site configurations are cracks, but if they are, then a crack capable of unstable crack growth would be about 60 mm (~ 2 inches) long, which is about two orders of magnitude larger than the estimated flaw size based on equivalent hydraulic diameter.
- A crack capable of unstable crack growth (i.e., a crack 60 mm long or longer) would have a leak rate of thousands of liters per day, which would be readily apparent.

The 3H Evaporator has a key role in SRS safely and timely reducing its 130 million liter liquid HLW waste inventory, closing remaining HLW tanks, and reducing the associated risks to workers, the public, and the environment. It also has engineered features that minimize the risks posed by these minor leaks. Operating the evaporator in a deliberate manner with enhanced surveillance appropriately balances the minimal risk posed by small, well-controlled releases of waste into the evaporator cell verses the potential long-term risks from extending storage in aging HLW tanks.

REFERENCES

1. D.P. CHEW and B.A. HAMM, *Liquid Waste System Plan Revision 20,* SRR-LWP-2009-00001, Revision 20, Savannah River Remediation, LLC, 2016. https://www.srs.gov/general/pubs/srr-lw-systemplan.pdf
2. SRR Fact Sheet, "Radioactive Liquid Waste Facilities," July 2017. http://www.srs.gov/general/news/factsheets/srr_rlwf.pdf
3. SRR Fact Sheet, "Evaporators Minimize Waste," February 2017. http://www.srs.gov/general/news/factsheets/srr_evaporators.pdf
4. C.F. JENKINS, "Performance of Evaporators in High Level Radioactive Chemical Waste Service," WSRC-TR-97-00297, CONF-980339, March 1998. https://www.osti.gov/servlets/purl/568436
5. T. YAMAMOTO, "Failure Evaluation of Savannah River Site High-Level Waste Evaporator 242-25H – Part I 17366," *WM2017 Conference, March 5-9, 2017, Phoenix, Arizona, USA*, March 2017.
6. C.H. KEILERS, B. WIERSMA, J. SCHWENKER, and T. YAMAMOTO, "Failure Evaluation of Savannah River Site High-Level Waste Evaporator 242-25H – Part II 17353," *WM2017 Conference, March 5-9, 2017, Phoenix, Arizona, USA*, March 2017.
7. J. GREGORY, K. RUDD, T. YAMAMOTO, W. BARNES, "Remote Evaporator Vessel Repair by Robotics and Powder Injection Laser Welding - 18107," *WM2018 Conference, March 18-22, 2018, Phoenix, Arizona, USA*, March 2018.
8. C.H. KEILERS, T. YAMAMOTO, and B. WIERSMA, "Failure Evaluation of Savannah River Site High-Level Waste Evaporator 242-25H – 18480," *WM2018 Conference, March 18-22, 2018, Phoenix, Arizona, USA*, March 2018.
9. HODGES, B.C., "Replacement of Melter 2 at the Defense Waste Processing Facility (DWPF) – 18608," *WM2018 Conference, March 18-22, 2018, Phoenix, Arizona, USA*, March 2018.
10. G.T. CHANDLER, R.L. SINDELAR, N.K. GUPTA, J.I., MICKALONIS, "Corrosion Performance of Alloy G3 and 304L Stainless Steel in Simulated High Level Waste Evaporator Solutions and Assessment of Service Life of Evaporator Tubes (U)," WSRC-MS-95-0470, March 1996.
11. G.T. CHANDLER, P.E. ZAPP, and J.I. MICKALONIS, "Hot-Wall Corrosion Testing of Simulated High Level Nuclear Waste (U)," WSRC-MS-94-0367, March 26-31, 1995.
12. Special Metals Corporation, "High-Performance Alloys for Resistance to Aqueous Corrosion," SMC-026, 2013. http://www.parrinst.com/wp-content/uploads/downloads/2011/07/Parr_Inconel-Incoloy-Monel-Nickel-Corrosion-Info.pdf
13. API 579-1/ASME FFS-1, *Fitness for Service*, June 2016.
14. ANDERSON, T.L., *Fracture Mechanics,* 3rd Edition, CRC Press, 2005.
15. ANDERSON, T.L. and D.A. OSAGE, "API 579: A Comprehensive Fitness-for-Service Guide," *International Journal of Pressure Vessels and Piping*, 77, pp953-963, 2000.
16. DEN HARTOG, J.P., *Advanced Strength of Materials,* McGraw-Hill, 1952.
17. TIMOSHENKO, S. and S. WOINOWSKY-KRIEGER, *Theory of Plates and Shells,* 2nd Edition, McGraw-Hill, 1959.
18. ASME Boiler and Pressure Vessel Code, Section VIII, Division I, 2015.
19. ROHENOW, W.M. and H. CHOI, *Heat, Mass, and Momentum Transfer,* McGraw-Hill, 1961.
20. FOX, R.W. and A.T. McDONALD, *Introduction to Fluid Mechanics*, 3rd Ed. Wiley, 1985.

ACKNOWLEDGEMENT

The author gratefully acknowledges inputs and insights from William Barnes (SRR), Eric Barrowclough (SRR), P.S. Lam (Savannah River National Laboratory), Phillip Norris (SRR), Bruce Wiersma (Savannah River National Laboratory), and Thomas Yamamoto (SRR).